Available online at www.sciencedirect.com
SCIENCE DIRECT®
Journal of Power Sources 138 (2004) 86–93
JOURNAL OF POWER SOURCES
www.elsevier.com/locate/jpowsour

Thermally nitrided stainless steels for polymer electrolyte membrane fuel cell bipolar plates Part 1: Model Ni–50Cr and austenitic 349™ alloys

H. Wang[a], M.P. Brady[b], G. Teeter[a], J.A. Turner[a,*]

[a] *National Renewable Energy Laboratory, Golden, CO 80401, USA*
[b] *Oak Ridge National Laboratory, Oak Ridge, TN 37831-6115, USA*

Received 17 May 2004; accepted 8 June 2004
Available online 11 September 2004

Abstract

Thermal nitridation of a model Ni–50Cr alloy at 1100 °C for 2 h in pure nitrogen resulted in the formation of a continuous, protective CrN/Cr_2N surface layer with a low interfacial contact resistance. Application of similar nitridation parameters to an austenitic stainless steel, 349™, however, resulted in a discontinuous mixture of discrete CrN, Cr_2N and $(Cr,Fe)_2N_{1-x}$ (x = 0–0.5) phase surface particles overlying an exposed γ austenite-based matrix, rather than a continuous nitride surface layer. The interfacial contact resistance of the 349™ was reduced significantly by the nitridation treatment. However, in the simulated PEMFC environments (1 M H_2SO_4 + 2 ppm F^- solutions at 70 °C sparged with either hydrogen or air), very high corrosion currents were observed under both anodic and cathodic conditions. This poor behavior was linked to the lack of continuity of the Cr-rich nitride surface formed on 349™. Issues regarding achieving continuous, protective Cr-nitride surface layers on stainless steel alloys are discussed.

Keywords: Thermal nitridation; Ni-based alloy; Stainless steel; PEMFC; Bipolar plate; Corrosion

1. Introduction

The polymer electrolyte membrane fuel cell (PEMFC) is a clean energy conversion device and is of great interest for both transportation and stationary power sources [1]. However, the high cost of its components, especially bipolar plates, restricts the wide application of PEMFCs. The bipolar plates connect the anode of one cell to the cathode of the next cell in a stack to achieve the required voltage. They also serve to distribute reactant and product gas flow streams. Stainless steels, which can significantly reduce cost relative to the traditionally used machined graphite plates, have been shown as possible candidate materials [2–6]. However, in PEMFC environments (especially under cathodic conditions), a passive film is formed on most stainless steels that are thicker than the air-formed native oxide film [7]. Although this passive film can protect the substrate stainless steel from further corrosion, higher electrical contact resistance is associated with this film [6,8], which can result in degradation in fuel cell performance. Further, under some fuel cell operating conditions, particularly at the anode, dissolution of metallic ions can result in contamination of the polymer membrane, which also degrades cell performance [9,10].

Recently, it was determined that thermally grown Cr nitrides (CrN/Cr_2N) on a model Cr-bearing alloy, Ni–50Cr (wt.%), show great promise in PEMFC bipolar plate environments [11,12]. The nitrided Ni–50Cr exhibited a stable and very low interfacial contact resistance and little metallic ion dissolution over the course of a 4000 h corrosion exposure under simulated PEMFC anodic and cathodic operating conditions and a 1000 h single-cell fuel cell test operated at 0.7 V [13]. This alloy is, however, too expensive for many PEMFC applications. The goal of the present work was to evaluate the

* Corresponding author. Tel.: +1 303 275 4270; fax: +1 303 275 3033.
E-mail address: john_turner@nrel.gov (J.A. Turner).

0378-7753/$ – see front matter © 2004 Elsevier B.V. All rights reserved.
doi:10.1016/j.jpowsour.2004.06.067

properties of similarly nitrided conventional stainless steel alloys for use as PEMFC bipolar plates. Part 1 of this paper presents results of electrochemical and interfacial contact resistance studies for an austenitic stainless steel, 349^{TM}, relative to nitrided Ni–50Cr (as a control). Part 2 presents results for a nitrided superferritic stainless steel, AISI446 mod 1.

2. Experimental

2.1. Material

Stainless steel plates of 349^{TM} were provided by J&L Specialty Steel, Inc. This grade of steel was selected due to its already promising performance in simulated PEMFC environments [6]. The nominal composition is: 0.05C, 23.0Cr, 14.5Ni, 1.5Mn, 1.4Si, 0.13N, 0.40Nb (wt.%), balance Fe. Alloy plates were cut into samples of 2.54 cm × 1.27 cm (1.0 in. × 0.5 in.). The samples were polished with #600 grit SiC abrasive paper, rinsed with acetone and dried with nitrogen gas. Comparable coupons of Ni–50Cr were made by arc-casting (details are presented in references [11–13]).

Initial optimization studies identified nitridation at 1100 °C for 1–2 h in pure nitrogen as yielding the most corrosion-resistant surface on the model Ni–50Cr alloy [11,12]. The thermal nitridation was accomplished in an alumina high-vacuum furnace. High purity nitrogen was purged and backfilled at a pressure of 1 atm. The nitrogen flow was stopped and the samples were heated to 1100 °C and held for 2 h for Ni–50Cr and for 2–7 h for 349^{TM}, followed by furnace cooling. The longer nitridation times used for the 349^{TM} reflect its moderately slower nitridation kinetics under these conditions. Nitrogen uptake was 1.9–2.3 mg cm^{-2} for Ni–50Cr, 1–1.1 mg cm^{-2} for 349^{TM} (2 h), and 2.3–2.7 mg cm^{-2} for 349^{TM} (7 h).

2.2. Microstructural characterization

Details of the microstructural characterization of the thermally nitrided Ni–50Cr are presented elsewhere [11–13]. The structure of the thermally nitrided 349^{TM} was investigated by means of X-ray diffraction (XRD), Auger electron spectroscopy (AES), and scanning electron microscopy (SEM) combined with energy dispersive X-ray spectroscopy (EDS). The XRD was conducted using a four-circle Scintag X-1 diffractometer (ThermoLab) with a Cu Kα anode source at a scanning speed of 0.03 degree per min. Glancing angle XRD technique was also used to investigate the structure of the near-surface layers (0.02 degree per step and a preset time of 3 s per step). AES was used to identify the nitride layer's composition and to determine the depth profile, using a Phi670 Auger Nanoprobe. The chamber base pressure was 3 × 10^{-10} Torr. The depth profiles were obtained by sputtering with 3 keV argon ions and a current density of around 1 μA mm^{-2}. During the sputtering, the system pressure in the chamber was approximately 5 × 10^{-8} Torr. Based on previous measurements, a reasonable estimate of the sputtering rate was approximately 80 nm min^{-1}.

2.3. Interfacial contact resistance

Interfacial contact resistance (ICR) measurements were carried out with metallic and as-nitrided samples at room temperature. Two pieces of conductive carbon papers were sandwiched between the sample and two copper plates. A current of 1.000 A was provided via the two copper plates and the total voltage drop was registered. While the compaction force was increased gradually, the total resistance dependency on the compaction force could be calculated. Similarly, the ICR value of the carbon paper/copper plate interface ($R_{C/Cu}$) was compensated by a calibration. Therefore, only the ICR values of carbon paper/nitride layer interface are reported. Further details of this technique are provided in reference [6].

2.4. Electrochemistry

Electrode contact with the nitrided alloy coupons was made by connecting one side of the sample to a copper wire by means of silver paint. The side for electrical conduction (backside) and the edges of the samples were mounted with epoxy, leaving the other side for electrochemical measurements. The sealing process was repeated to eliminate possible leakage. Details of the procedure can be found elsewhere [6].

To simulate an aggressive PEMFC environment, a 1 M H_2SO_4 + 2 ppm F^- solution at 70 °C [5,14] was used, bubbled thoroughly either with hydrogen gas (for simulating the PEMFC anode environment) or pressured air (for simulating the PEMFC cathode environment) prior to and during the electrochemical measurements. The solution was bubbled at least 20 min before starting the experiment. Aconventional three-electrode system was used in the electrochemical measurements, in which a platinum sheet acted as the counter electrode and a saturated calomel electrode (SCE) was used as the reference electrode. The potentials reported are relative to SCE unless noted otherwise. A Solartron 1287 potentiostat interfaced to a computer was used to conduct the electrochemical experiments. Dynamic polarization technique was used to compare the general electrochemical behavior of the nitrided coupons. In these tests, the samples were stabilized at open circuit potential (OCP) for 5 min. The potential was then swept from the OCP in the anodic direction with a scanning rate of 1 mV s^{-1}. Potentiostatic polarization experiments were also conducted to investigate the corrosion resistance and stability of the nitride layer under PEMFCs' operation conditions. In these measurements, samples were stabilized at OCP for 5 min, then a specific potential was applied and the current–time curve was registered. Two potentials were chosen for the tests: −0.1 V (equivalent to ∼0.1 V_{NHE}) [15] for the simulated PEMFC

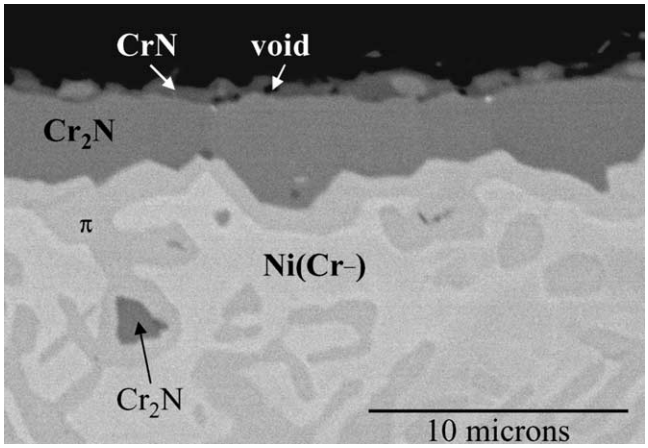

Fig. 1. SEM cross-section showing typical microstructure of nitrided Ni–50Cr (wt.%) after 1–2 h at 1100 °C in pure nitrogen [11]. Ni(Cr-) refers to Cr-depleted Ni(Cr) relative to the bulk alloy concentration of Cr.

anode environment where the solution was sparged with hydrogen gas, and 0.6 V (which is equivalent to ~0.8 V_{NHE}) for the simulated PEMFC cathode environment where the solution was sparged with air. Corrosion current densities of the order of 10^{-6} A cm^{-2}, under these conditions, are considered sufficiently promising to warrant long-term corrosion testing and single-cell fuel cell testing. It should be emphasized that such polarization studies are a screening technique and the 10^{-6} A cm^{-2} corrosion current density goal is merely a rough guideline to gage-expected fuel cell behavior, rather than a well-established property target. The key issue is the extent to which the corrosion processes would be detrimental in the actual PEMFC bipolar plate environments, i.e. increased contact resistance or metallic ion dissolution and membrane poisoning.

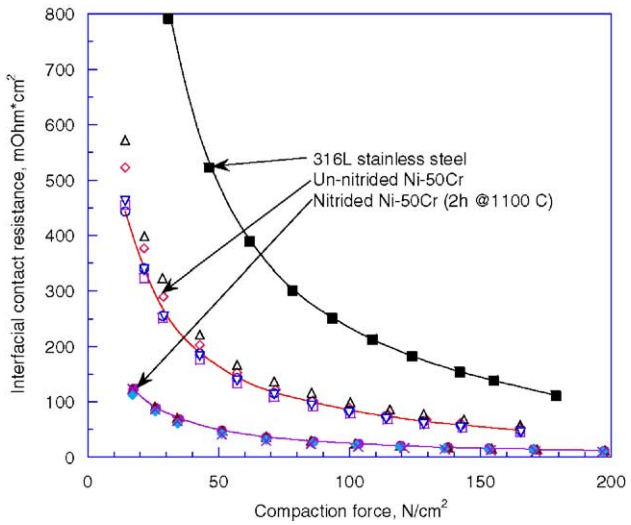

Fig. 2. Interfacial contact resistance for non-nitrided and nitrided Ni–50Cr alloy as a function of compaction force. Data for 316L are shown for comparison.

3. Results and discussion

3.1. Nitrided Ni–50Cr control

A typical microstructure of Ni–50Cr nitrided at 1100 °C for 1–2 h in pure nitrogen is shown in Fig. 1. It consisted of a nearly continuous ~1 μm thick layer of CrN overlying a dense, continuous 3–5 μm thick layer of Cr_2N. Underlying the Cr_2N layer was a continuous layer of the ternary Cr–Ni–N π phase, and an internally nitrided zone of π phase intermixed with Cr-depleted Ni(Cr-) metal. Total nitrogen uptake was on the order of 1.9–2.3 mg cm^{-2}, with a substantial portion of the nitrogen incorporated into the internally nitrided zone.

ICR data as a function of compaction pressure are shown in Fig. 2. The Ni–50Cr alloy (no nitridation treatment) had a lower contact resistance than 316L stainless steel, shown for comparative purposes. Subsequent nitridation of

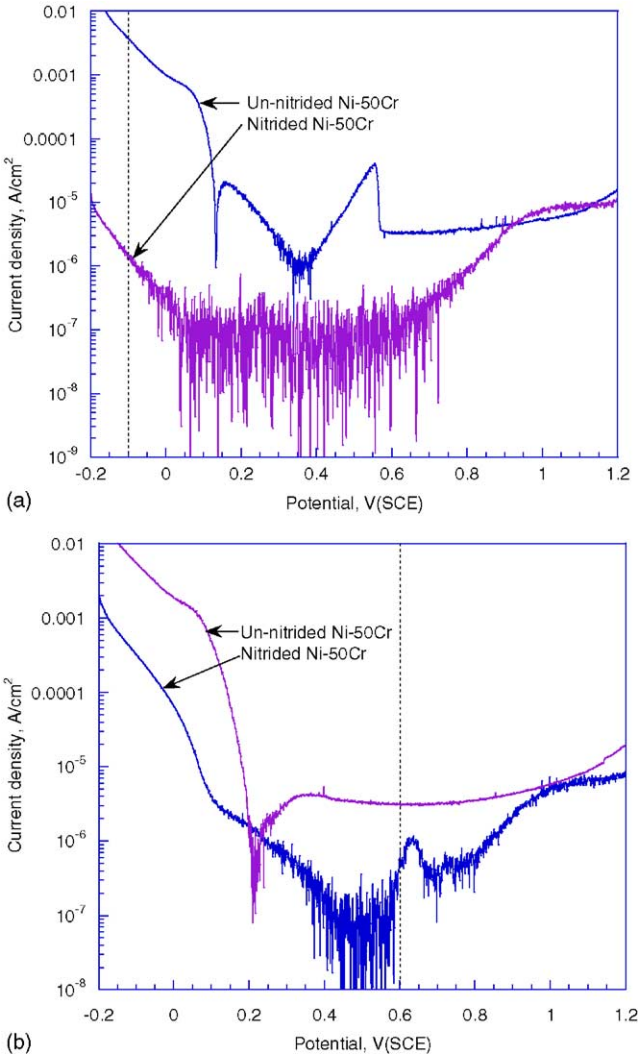

Fig. 3. Anodic behavior of non-nitrided and 2 h nitrided Ni–50Cr alloy in 1 M H_2SO_4 + 2 ppm F^- at 70 °C. The solution was sparged either with hydrogen gas (a) or air (b). The scanning rate was 1 mV s^{-1}. The anode and cathode operation potentials in a PEMFC are marked.

Ni–50Cr significantly lowered the contact resistance, especially at the low compaction forces relevant to PEMFC stacks (∼100–150 N cm $^{-2}$ range) (Fig. 2).

In the 1 M H_2SO_4 + 2 ppm F^- solution at 70 °C, anodic polarization curves for Ni–50Cr and nitrided Ni–50Cr showed a significant decrease in corrosion currents under H_2-purged (anodic) conditions and air-purged (cathodic) conditions for the samples undergoing the nitridation treatment (Fig. 3). Additionally, the OCP under cathodic conditions was raised from ∼0.2 V for Ni–50Cr metal to ∼0.5 V for nitrided Ni–50Cr, Fig. 3b. A similar comparison for anodic conditions was not possible due to the very low corrosion currents and correspondingly high level of noise for the nitrided Ni–50Cr sample. However, potentiostatic polarization data for nitrided Ni–50Cr in the H_2 purged anodic environment held at −0.1 V for 4–6 h showed a stable cathodic current in the range 3–4 × 10^{-6} A cm^{-2}, which is consistent with protective behavior, not dissolution (Fig. 4a). No increase in ICR was associated with this polarization behavior (Fig. 4b). The results of these electrochemical and contact resistance studies were therefore consistent with the excellent behavior exhibited by nitrided Ni–50Cr in the long-term corrosion testing and single-cell fuel cell testing reported previously [13].

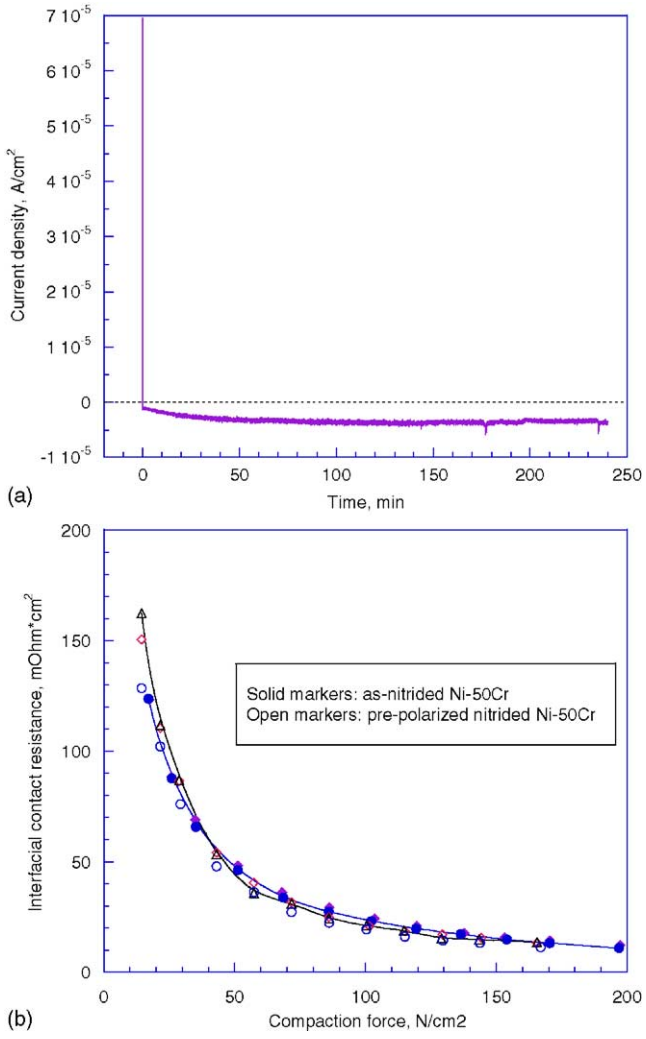

Fig. 4. (a) Behavior of the 2 h nitrided Ni–50Cr alloy at −0.1 V in 1 M H_2SO_4 + 2 ppm F^- at 70 °C with the solution sparged with hydrogen gas, (b) influence of polarization on the interfacial contact resistance of nitrided Ni–50Cr alloy.

3.2. *Nitrided 349^{TM} stainless steel*

3.2.1. *Microstructure*

XRD indicated the presence of Cr_2N, $(Cr,Fe)_2N_{1-x}$ (x = 0–0.5), CrN, and γ austenite phases for 349^{TM} after nitridation at 1100 °C in pure N_2. The diffraction patterns after 2 and 7 h of nitridation were nearly identical, except that the relative intensities of the CrN peaks were moderately higher in the 7 h sample. To more definitively investigate the structure of the outermost regions of the nitrided surface of 349^{TM}, glancing angle XRD was carried out with the 7 h nitrided sample (Fig. 5). The austenite peak of γ[2 0 0] disappeared when the grazing angle was decreased below 2°, suggesting that the outmost surface layer was nitrided and did not contain significant amounts of γ. The overlapping peaks of CrN[2 0 0] and γ[1 1 1] also decreased to a low level at grazing angle below 2°, in agreement with the aforementioned change in γ[2 0 0]. At a grazing angle of 0.2°, considered representative of the outermost surface region, the data suggest that CrN, Cr_2N and $(Cr,Fe)_2N_{1-x}$ phases were all present.

An SEM surface micrograph of 7 h nitrided 349^{TM} is shown in Fig. 6a. Based on EDS analysis, the surface consisted of discrete particles of a Cr-rich nitride phasecontaining a minor amount of Fe, overlying a matrix of a Fe–Cr-rich region. Cross-sectional analysis confirmed the lack of continuity of the Cr-rich nitride surface particles (Fig. 6b). The contrast evident in the cross-section image of the

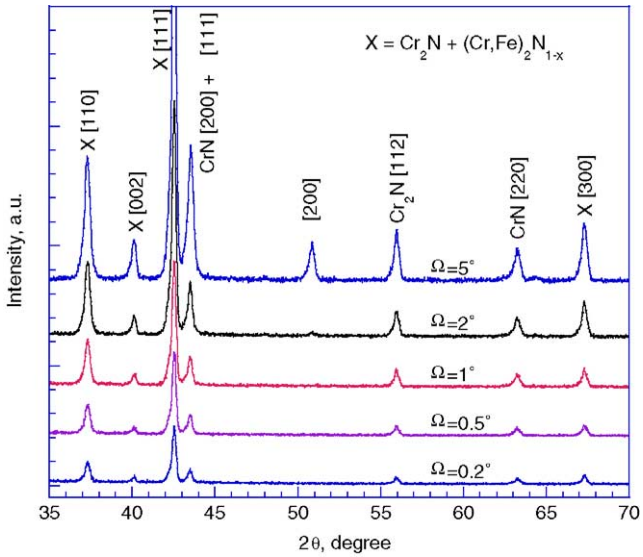

Fig. 5. Glancing angle XRD patterns for 7 h thermally nitrided 349^{TM} stainless steel. In general, peak intensity decreases with decreasing grazing angles.

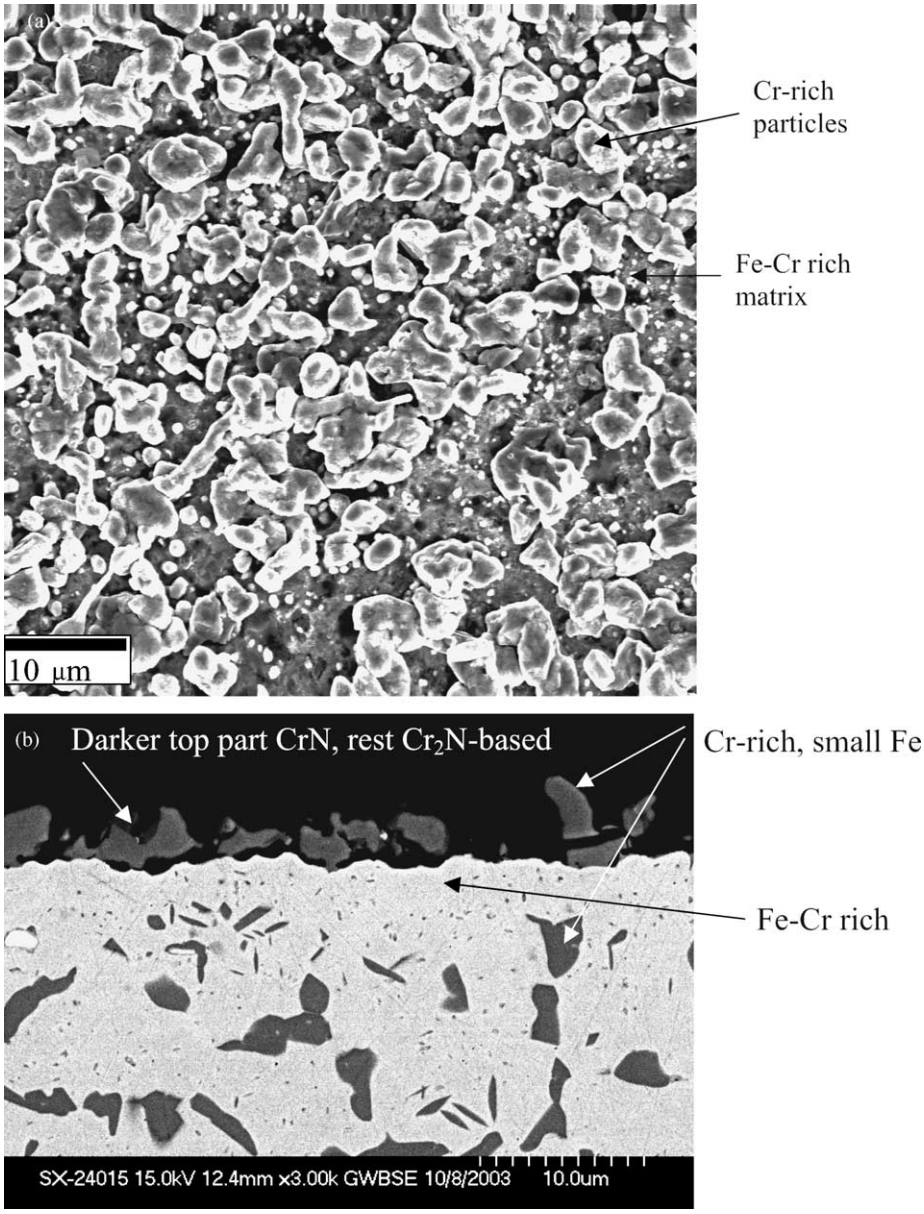

Fig. 6. SEM images of thermally nitrided 349^{TM} stainless steel. (a) Top view, (b) cross-section view.

surface particles suggests that many were not homogeneous, but rather contained thin surface patches of a more nitrogen rich (darker) Cr-nitride phase. The underlying Fe–Cr-rich matrix phase contained discrete internal Cr-rich nitride precipitates, of similar nominal composition to those observed at the surface, except that the patches of the darker Cr-nitride phase were not observed. In light of the XRD data, the discrete Cr-rich nitride surface particles are likely Cr_2N and, possibly, $(Cr,Fe)_2N_{1-x}$, with thin patches of CrN at the outermost surface. The Fe–Cr-rich matrix phase was γ austenite containing internal $Cr_2N/(Cr,Fe)_2N_{1-x}$ precipitates. The outermost surface of the γ austenite matrix phase may also be nitrogen-rich, possibly as a thin layer of $(Cr,Fe)_2N_{1-x}$ and/or with N dissolved in solution.

An AES depth profile of the 7 h nitrided steel is shown in Fig. 7a. Interpretation of this data is complicated by the heterogenous nature of the surface (Fig. 6a) relative to the AES sampling area of approximately 1 mm^2. It is seen that the surface layer was composed mainly of Cr, N and Fe, with a minor amount of oxygen. Little Ni was observed at the surface. Oxygen in the nitride layer is not surprising, since a native oxide film existed on the stainless steel prior to nitridation and there may be some oxygen impurities initially present in the input nitrogen gas used for the nitridation process. (Occasional isolated discrete Cr_2O_3 particles were observed in the nitride layer formed on Ni–50Cr [13]).

It is interesting to note that two peaks for Fe could be registered from the analysis of the data, one for metallic Fe

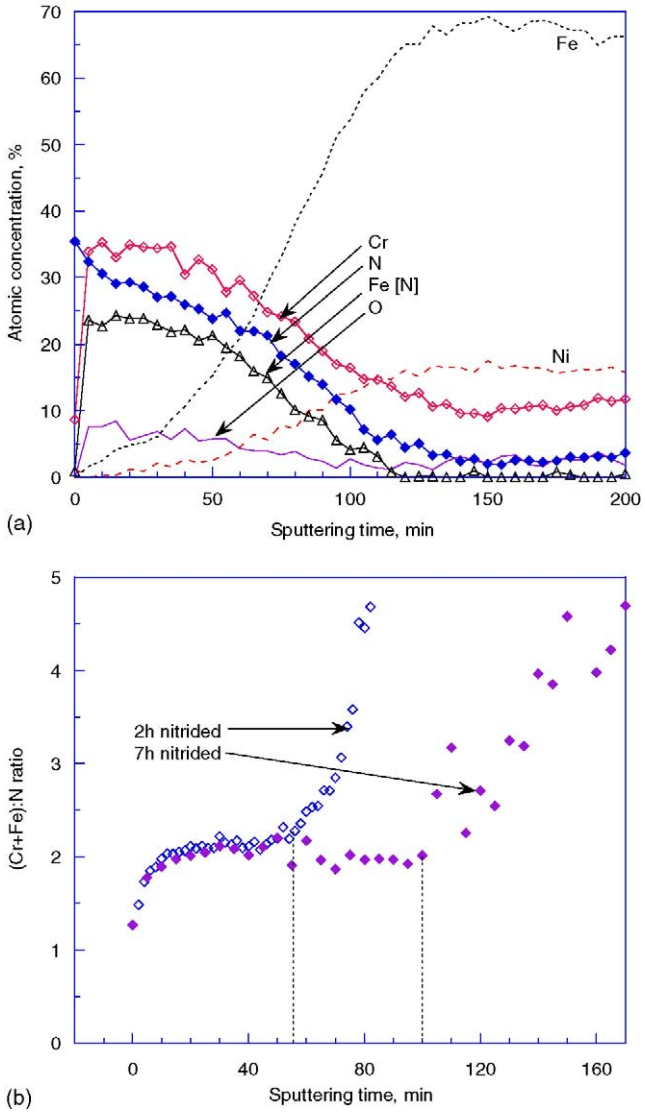

Fig. 7. AES depth profile of thermally nitrided 349^{TM} stainless steel (a), and the [Cr+Fe(N)]:N ratio (b).

and the other associated with nitrogen, designated Fe[N] in Fig. 7. This is likely the Fe associated with the $(Cr,Fe)_2N_{1-x}$ phase detected by XRD. The [Cr+Fe(N)]:N ratio dependency on the sputtering time is shown in Fig. 7b. The [Cr+Fe(N)]:N ratio increased with increasing sputtering time, from close to 1 at the outermost surface to a plateau region of 2 through much of the nitrided zone. This is consistent with the detection of CrN by XRD and the SEM cross-section at the outermost surface of the discrete $Cr_2N/(Cr,Fe)_2N_{1-x}$ surface particles.

3.2.2. *Interfacial contact resistance*

Interfacial contact resistance for both 2 h and 7 h nitrided 349^{TM} stainless steel was investigated as a function of compaction force (Fig. 8). Very low ICR values were obtained. For comparison, the inset of Fig. 8 gives the ICR values obtained under the same condition for metallic 349^{TM} samples.

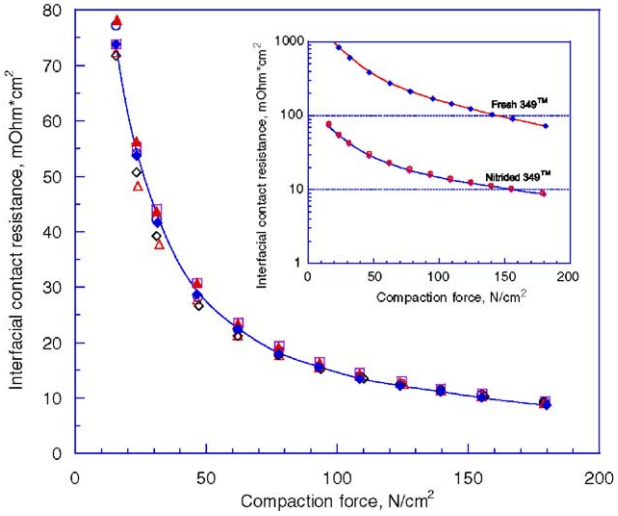

Fig. 8. Interfacial contact resistance for thermally nitrided 349^{TM} steel and carbon paper at different compaction forces. The inset compares the interfacial contact resistance of the fresh 349^{TM} steel sample and the thermally nitrided ones. Solid markers are for 2 h nitrided samples and open markers are for 7 h nitrided ones.

ICR values for nitrided steel were approximately one decade lower than those of bare metal, illustrating the beneficial effect of thermal nitridation on the surface conductivity of the steel. At a compaction force of around 150 N cm^{-2}, the ICR values are on the order of $\sim 100 \times 10^{-3}$ Ohm cm^2 for fresh 349^{TM} [6] and approximately 10×10^{-3} Ohm cm^2 for the nitrided 349^{TM}. This is attributed to a higher conductivity of the nitride phases over the native oxides that form on the alloy. It is also consistent with the lack of significant oxygen/oxide content evident in the AES analysis of the surface of the nitrided material.

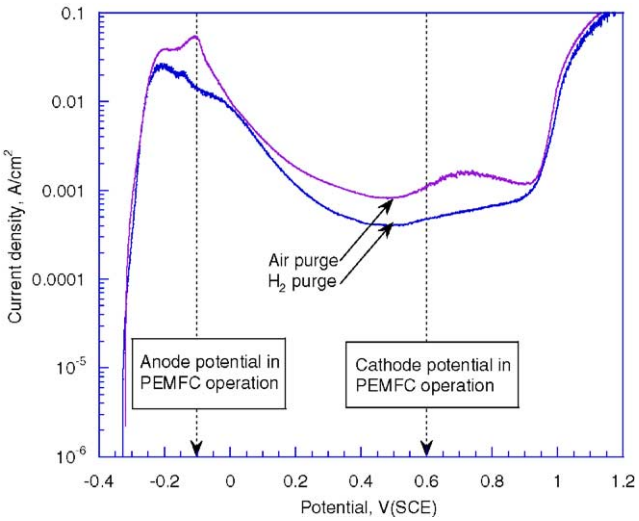

Fig. 9. Anodic behavior of 7 h thermally nitrided 349^{TM} steel in 1 M H_2SO_4 + 2 ppm F^- at 70 °C. The solution was sparged either with hydrogen gas or air. The scanning rate was 1 mV s^{-1}. The anode and cathode operation potentials PEMFC are marked.

3.2.3. Polarization

The anodic polarization curves of 7 h nitrided 349^{TM} steel in 1 M H_2SO_4 + 2 ppm F^- at 70 °C sparged either with hydrogen or air are shown in Fig. 9. Typical operating potentials in PEMFC's conditions, approximately −0.1 V for PEMFC anode environment and 0.6 V for PEMFC cathode environment according to [15], are marked in the figure. The nitrided 349^{TM} steel qualitatively behaves like the metallic (not nitrided) 349^{TM} steel [6], but with much higher corrosion currents, rather than lower currents as were observed for nitrided Ni–50Cr relative to metallic Ni–50Cr (Fig. 3). Regardless of the purging gases, very high anodic currents (on the order of 10^{-3} A cm^{-2}) were observed for the 7 h nitrided 349^{TM} steel in the whole potential range investigated. After the polarization, gray-dark "dusts" were noticed in the solution, a sign of the dissolution of the electrode. The lowest current in the passive region was ∼0.4 × 10^{-3} A cm^{-2} in H_2-sparged solution and ∼0.9 × 10^{-3}A cm^{-2} in the air-sparged solution. Trans-passivation started at ∼0.94 V in both solutions. The current densities at this level are orders of magnitude too high for the PEMFC bipolar plate application, as well as significantly higher than those observed for nitrided Ni–50Cr (Fig. 3).

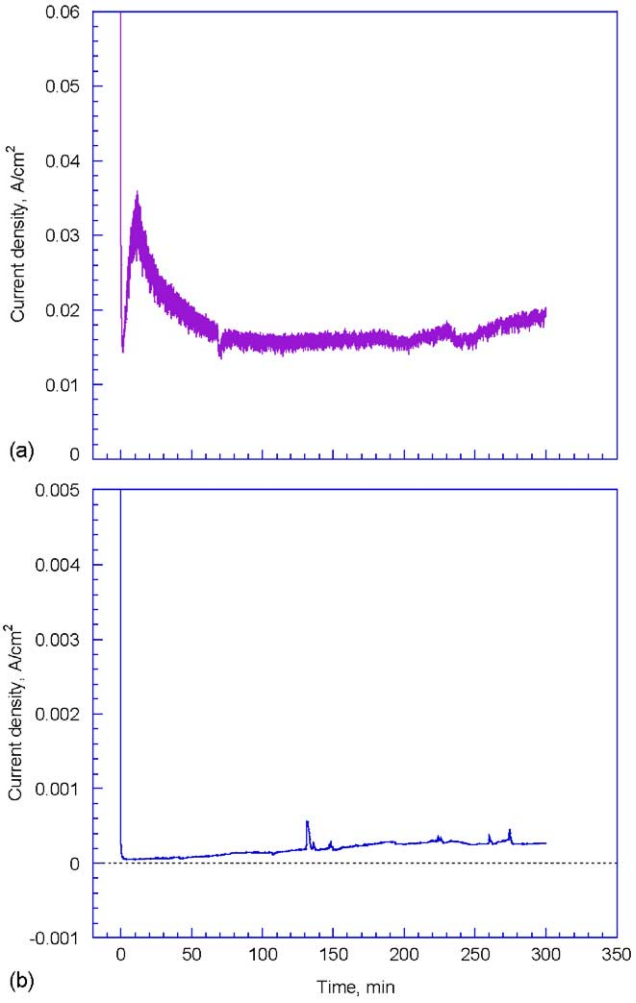

Fig. 10. Current–time behavior of the 7 h nitrided 349^{TM} steel at constant applied potentials: (a) obtained when the electrode was polarized at −0.1 V and the solution was sparged with hydrogen gas, (b) obtained when the electrode was polarized at 0.6 V and the solution was sparged with air.

To further investigate the behavior under simulated PEMFC conditions, potentiostatic polarization measurements were carried out either at −0.1 V for the solution sparged with hydrogen gas (anode conditions) and at 0.6 V for the solution sparged with air (cathode conditions; Fig. 10). In both cases, the transient current decays sharply at the beginning of polarization, then it stabilizes. When the nitrided steel was polarized at −0.1 V (Fig. 10a), a current peak of ∼35 × 10^{-3} A cm^{-2} appeared at ∼15 min polarization, followed by a secondary decay and stabilization. The stable current was ca. 15–20 × 10^{-3} A cm^{-2}. In the air-sparged simulated PEMFC cathode environment, the current decayed faster and was relatively more stable than in the simulated PEMFC anode environment, Fig. 10b. Although there was a tendency for a slow increase with prolonged polarization, a stable current of ∼0.25 × 10^{-3} A cm^{-2} was obtained. In the case of native (not nitrided) stainless steels, the fast decay of the current is generally related to the passive film formation process [6,7]. With the 1100 °C pure nitrogen nitrided 349^{TM} steel, current decay could be also related to this process. However, the very high current densities suggest a difficulty in formation of a protective passive film and/or the extensive oxidation/dissolution of the nitrided surface. The dust in solution by visual investigation after the polarization test is strong evidence of such dissolution.

4. Summary and conclusions

Thermal nitridation of 349^{TM} at 1100 °C in pure nitrogen resulted in a nitrided surface, composed of a mixture of CrN, Cr_2N and $(Cr,Fe)_2N_{1-x}$ (where x = 0–0.5) phases, in which Cr_2N and $(Cr,Fe)_2N_{1-x}$ were predominant. CrN was found on the outermost surface, overlying the $(Cr,Fe)_2N$ and Cr_2N. Due to the low electrical resistance of nitrides, the interfacial contact resistance was significantly reduced on nitridation, a key advantage for PEMFC stacks. However, polarization studies in simulated PEMFC environments indicated unacceptably high corrosion current densities as well as the anodic dissolution of the nitrided on 349^{TM}. In contrast, nitrided Ni–50Cr control coupons showed low contact resistance and low corrosion current densities under these conditions, consistent with the excellent single-cell fuel cell performance observed for this material [13].

The discrete nitride surface particles formed on 349^{TM} under the nitridation conditions and the potential for forming local galvanic cells with the underlying exposed substrate alloy, are considered the primary reasons for the poor corrosion resistance and extensive anodic dissolution observed under these simulated aggressive PEMFC environments. This resulted in significantly poorer corrosion resistance than that

in untreated 349^{TM}. The incorporation of significant quantities of substrate alloy Fe into the nitrided surface (Fig. 7) may also have contributed to the poor corrosion resistance. Nitridation of Ni–50Cr resulted in the formation of a continuous, dense surface of CrN/Cr_2N, without incorporation of Ni base metal into the surface of the nitrided region. It therefore might be necessary to modify the nitridation conditions and/or alloy composition of the austenitic stainless steels (such as 349^{TM}) to favor a continuous, exclusive Cr-nitride layer formation in order to achieve the necessary corrosion resistance for PEMFC bipolar plate applications. The morphology of the surface of the nitridated 349^{TM} steel, e.g. discrete surface nitride particles, suggests that the issues related to surface energy and nitride nucleation during the nitridation reaction will need to be addressed to achieve the desired results. These phenomena may be controlled by the modification of time, temperature, and nitrogen activity in the nitriding environment, possibly in combination with alloying to promote external, continuous nitride layer formation [13]. In particular, a wide range of nitriding activities can be achieved via N_2–H_2 mixtures, which may allow for a range of nitride morphologies to be synthesized.

Part 2 of this paper examines nitridation behavior of a high Cr, superferritic stainless steel, 446 mod 1. This alloy was more amenable to Cr-nitride layer formation, although a continuous layer was not achieved under the nitridation conditions studied. However, a new nitride-based surface modification phenomenon, which shows good promise for PEMFC bipolar plate applications, was observed.

Acknowledgements

The authors wish to thank Tracy Brummett for assisting in the SEM analysis. This work was supported by the Hydrogen, Fuel Cell and Infrastructure Technologies Program of the U.S. Department of Energy (DOE). Oak Ridge National Laboratory is managed by UT-Battelle, LLC for the US DOE under contract DE-AC05-00OR22725.

References

[1] B.C.H. Steele, A. Heinzel, Nature (London) 414 (2001) 345.
[2] R. Hornung, G. Kappelt, J. Power Sources 72 (1998) 20.
[3] R.C. Makkus, A.H.H. Janssen, F.A. de Bruijn, R.K.A.M. Mallant, J. Power Sources 86 (2000) 274.
[4] D.P. Davies, P.L. Adcock, M. Turpin, S.J. Rowen, J. Power Sources 86 (2000) 237.
[5] J. Scholta, B. Rohland, J. Garche, in: P.R. Roberge (Ed.), Proceedings of the 2nd International Symposium on New Materials for Fuel Cell and Modern Battery Systems, Ecole Polytechnique de Montreal, Canada, 1997, p. 300.
[6] Wang Heli, Mary Ann Sweikart, John A. Turner, J. Power Sources 115 (2) (2003) 243.
[7] H. Wang, G. Teeter, C. Jiang, J.A. Turner, On the Passivation of 349^{TM} Stainless Steel in a Simulated PEMFC Cathode Environment, submitted to Corros. Sci.
[8] H. Wang, J.A. Turner, Investigation of a duplex stainless steel as PEM bipolar plate material, J. Electrochem. Soc., in press.
[9] J. Wind, R. Spah, W. Kaiser, G. Bohm, Metallic bipolar plates for PEM fuel cells, J. Power Sources 105 (2) (2002) 256–260.
[10] M.C. Li, C.L. Zeng, S.Z. Luo, J.N. Shen, H.C. Lin, C.N. Cao, Electrochemical corrosion characteristics of type 316 stainless steel in simulated anode environment for PEMFC, Electrochim. Acta 48 (12) (2003) 1735–1741.
[11] M.P. Brady, K. Weisbrod, C. Zawodzinski, I. Paulauskas, R.A. Buchanan, L.R. Walker, Electrochem. Solid State Lett. 5 (2002) 245–247.
[12] M.P. Brady, I. Paulauskas, R.A. Buchanan, K. Weisbrod, H. Wang, L.R. Walker, L.S. Miller, Proceedings of the 2nd European PEFC Forum, Lucerne, Switzerland, 30 June, 2003.
[13] M.P. Brady, K. Weisbrod, I. Paulauskas, R.A. Buchanan, K.L. More, H. Wang, M. Wilson, F. Garzon, L.R. Walker, Scripta Mater. 50 (7) (2004) 1017.
[14] D. Chu, R. Jiang, J. Power Sources 80 (1999) 226.
[15] R.L. Borup, N.E. Vanderborgh, Materials Research Society Symposium Proceedings, Mater. Res. Soc. 393 (1995) 151.